ACS APPLIED MATERIALS & INTERFACES

Letter

www.acsami.org

Electrochemical Activity of Glucose Oxidase on a Poly(ionic liquid)–Au Nanoparticle Composite

Sungwon Lee, Bryan S. Ringstrand, David A. Stone,† and Millicent A. Firestone*

Materials Science Division, Argonne National Laboratory, 9700 South Cass Avenue, Argonne, Ilinois 60439, United States

Supporting Information

ABSTRACT: Glucose oxidase (GOx) adsorbed on an ionic liquid-derived polymer containing internally organized columns of Au nanoparticles exhibits direct electron transfer and bioelectrocatalytic properties towards the oxidation of glucose. The cationic poly(ionic liquid) provides an ideal substrate for the electrostatic immobilization of GOx. The encapsulated Au nanoparticles serve to both promote the direct electron transfer with the recessed enzyme redox centers and impart electronic conduction to the composite, allowing it to function as an electrode for electrochemical detection.

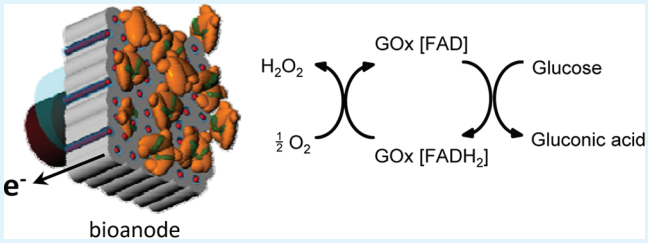

KEYWORDS: *bioanide, gold nanoparticles, direct electron transfer, enzymatic catalysis*

INTRODUCTION

The use of conducting polymers to either monitor or control biomolecules is becoming increasingly important, underpinning the emerging field of biocommunication.[1−3] Conducting polymers offer several noted advantages over conventional electrode materials (metals and semiconductors), including the possibility to function as a molecular wire to a protein redox center. Other benefits include mechanical properties matched to the protein, chemical composition that promotes electrostatic binding of the enzyme, and fabrication of the polymer into a variety of 3D forms for increased protein loading.[4] Significant opportunities exist for designing conductive biocompatible polymers that can embody these characteristics and serve as an efficient electrical conduit (organic electrode) to enable communication with a variety of biomolecules, such as oxidoreductases. Oxidoreductases are abundant proteins in nature that catalyze the transfer of electrons. Their catalytic activity makes them ideal candidates for use in the construction of a variety of biodevices, including batteries, fuel cells or electronics.[5] Realization of such biodevices, however, requires achieving efficient electronic coupling between the protein redox center and the electrode.[6] Inefficient electron conduction between enzyme and electrode arises primarily from the recessed redox centers of the protein. Although small redox mediators are commonly used to facilitate electrical communication, acting to shuttle electrons between the enzyme and the electrode surface,[7,8] they suffer from poor retention and slow diffusion. Moreover, soluble mediators cannot be readily used in solid-state devices. Direct electron transfer (DET) achieved by appropriate immobilization and/or electrical "wiring" of the enzyme onto the electrode can obviate the need for small diffusing mediators. Numerous approaches for promoting DET have been reported,[9] including reconstitution of linker modified cofactors,[9,10] co-entrapment with redox molecules (osmium complex functionalized polymer)[9] and integration with nanomaterials (e.g., Au nanoparticles[10] and carbon nanotubes).[11,12] Preparation of enzyme-electron relay conjugates often requires elaborate, multistep syntheses. Thus, there is an ongoing need for further advancement of materials and approaches for facile electrical coupling of enzymes with electrodes.

Polymeric ionic liquids (poly(IL)s) prepared by the polymerization of ionic liquid monomers could offer an ideal platform for further development as biocompatible conduits.[13,14] The potential utility of poly(IL)s lies in the established tunability of the molecular structure of ionic liquids, leading to exquisite control over their physicochemical properties, in combination with the advantages of polymers: stability, processability and durability. Recently, two approaches for the introduction of electronic transport into polymerized ionic liquids have been described.[15−17] The first incorporated a π-conjugated moiety into the IL monomer, which was then polymerized into a highly structured conducting polymer.[15] In a second approach, metal nanoparticles (NPs) were synthesized during photopolymerization of the self-assembled lyotropic IL mesophase.[16,17] The latter approach yielded a bulk, multidimensional Au NP-polymer composite possessing 1-D columns of packed spherical Au NPs within hexagonally ordered hydrophilic pores of a perforated lamellar structured polymerized ionic liquid.[16,17] The internally ordered columnar arrangement of Au spherical NPs functions as an electronic conduction pathway.[17] Herein, we evaluate the use of the Au NP−poly(IL) composite as a novel platform for biocommunication, functioning both as the electrode material and to

Received: January 5, 2012
Accepted: May 1, 2012
Published: May 1, 2012

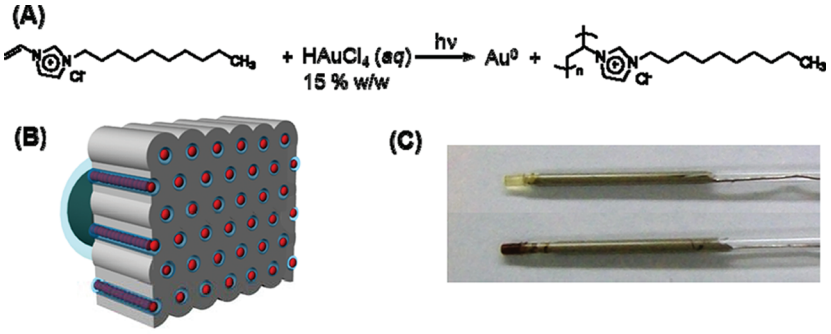

Figure 1. (A) Synthetic scheme for the preparation of the Au-poly[$C_{10}VIm^+$][Cl^-] composite. (B) Schematic illustration of Au-poly[$C_{10}VIm^+$][Cl^-] composite based on previously published SAXS and AFM structural characterization.[16,17](C) Photographs of fabricated electrodes of poly[$C_{10}VIm^+$][Cl^-] composite without (top) and with Au nanoparticles (bottom).

facilitate direct electron transfer with a model oxidoreductase, glucose oxidase, GOx.

EXPERIMENTAL SECTION

Materials and Methods. All chemicals were purchased from Sigma-Aldrich (Milwaukee, WI) and used as received unless otherwise noted. 1-Chlorodecane and 1-vinylimidazole were distilled under reduced pressure then collected and stored under a blanket of nitrogen and in the absence of light. Nanopure water was obtained from Barnstead E-pure water purifier (18 MΩ·cm). Absolute ethanol (200 proof) was purchased from Pharmco-aaper (Brookfield, CT).

Monomer and Polymer Synthesis. *1-Decyl-3-vinylimidazolium Chloride, [$C_{10}VIm^+$][Cl^-].* A solution of freshly distilled 1-vinylimidazole (6.4 mL, 70.5 mmol) and 1-chlorodecane (2.9 mL, 14.1 mmol) in anhydrous CH_3CN (25 mL) was heated at 80 °C for 72 h under Ar in the dark. The light orange solution was cooled down to 21°C and filtered to remove insoluble particulates. Excess CH_3CN was removed in vacuo (no more than 40 °C), and the resulting light orange viscous oil was suspended in Et_2O. The biphasic mixture was vigorously stirred for 15 min, and the Et_2O was decanted. The process was repeated until the viscous oil crystallized. The product was isolated by filtration and dried under vacuum overnight giving 2.66 g (70 % yield) as white crystals. ^1H NMR ($CDCl_3$) δ: 0.86 (t, J = 7.0 Hz, 3H), 1.20-1.39 (m, 14H), 1.95 (quint, J = 6.1 Hz, 2H), 4.37 (t, J = 7.5 Hz, 2H), 5.37 (dd, J_1 =8.7 Hz, J_2 = 3.0 Hz, 1H), 5.95 (dd, J_1 = 15.7 Hz, J_2 = 3.0 Hz, 1H), 7.42 (t, J = 1.7 Hz, 1H), 7.54 (dd, J_1 = 15.7 Hz, J_2 = 8.7 Hz, 1H), 7.76 (t, J = 1.8 Hz, 1H), 11.4 (s, 1H); ^{13}C NMR ($CDCl_3$) δ: 14.1, 22.6, 26.2, 28.9, 29.2, 29.3, 29.4, 30.2, 31.8, 50.4, 109.4, 118.6, 122.0, 128.5, 137.3.

Gold-Incorporated Poly(1-decyl-3-vinylimidizolium Chloride), Au-poly[$C_{10}VIm^+$][Cl^-]. A typical polymerization is as follows: Water content of the monomer was determined by TGA to be ~3 wt %. 1-Decyl-3-vinylimidizolium chloride (107 mg) was treated with 0.1 M $HAuCl_4$ (16.0 μL) producing a final water content of 15 % w/w. The mixture was heated to 75 °C in a capped vial and repeatedly vortex mixed until homogeneous. The bright yellow solution was drawn into the tip of pre-heated (with heat gun) borosilicate pipet and sealed at the narrow end. Care was taken to prevent air bubbles from entering the pipet to ensure a continuous sample. To initiate polymerization, the pipet was placed 2 inches away from a high intensity UV light source (λ = 254 nm; Hanovia 400 W mercury arc lamp) for 2 h. The sample was rotated 180° midway through the polymerization.

Physical Methods. High-field ^1H (500.13 MHz) and ^{13}C (125.76 MHz) NMR spectra were obtained using a Bruker AMX-500 spectrometer. ^1H and ^{13}C NMR spectra were referenced to $CDCl_3$ at 7.24 and 77.0 ppm, respectively. ATR/FT-IR spectroscopy was performed using a Bruker Vertex 70 spectrometer over the frequency range 4000-700 cm^{-1} with spectra recorded at 4 cm^{-1} resolution and averaged over 256 scans. Thermogravimetric analysis (TGA) was carried out using a TA Instrument Q50 by heating a known amount of sample (10-15 mg) in a platinum pan from 20 °C to a final temperature of 500 °C at a rate of 10 °C/min under N_2 flow. Fluorescence spectroscopy was performed using PTI spectrofluorometer (Birmingham, NJ). All electrochemical measurements were performed using a conventional three-electrode set-up (BAS EC Epsilon potentiostat/galvanostat, West Lafayette, IN) equipped with C-3 cell stand. Ag/AgCl electrode (saturated KCl) and a platinum wire were employed as reference and counter electrode, respectively. The fabricated electrodes were used as the working electrode.

Electrode Fabrication. Au-poly[$C_{10}VIm^+$][Cl^-] electrodes were cut with cylindrical dimensions of ca. 1 mm dia. × 3 mm length and inserted into a thoroughly cleaned (ethanol, water and dried) borosilicate glass capillary (ca. 1 mm dia. × 5 cm length). Electrical connection was achieved by insertion of a tinned copper wire (ca. 10 cm length) into the glass capillary and filled with silver colloidal paste (Ted Pella Inc, Redding, CA). The electrode was sealed using an adhesive (Duco cement, ITW Devcon, Wooddale, IL) and cured completely before use. The resulting electrodes have a surface area of ca. 0.046 cm^2. Glucose oxidase was immobilized on the fabricated electrodes by immersion into 10 mg/mL GOx in 10 mM phosphate buffer saline (pH 7.4) overnight at 4 °C. Electrodes were stored at 4 °C.

Enzyme Assay. GOx was stripped from the Au-poly[$C_{10}VIm^+$][Cl^-] electrode by immersing in 8 M urea/10 mM phosphate buffer (pH 7.4) for 2 h. Fluorescence measurements were performed with an excitation wavelength of 375 nm, and the emission was recorded between 450 and 650 nm (0.25 nm resolution). A calibration curve was obtained from standard solutions of FAD (35−880 nM in 8 M urea/10 mM phosphate buffer, pH 7.4).

RESULTS AND DISCUSSION

The Au NP-poly(IL) composite, Au-poly[$C_{10}VIm^+$][Cl^-] was synthesized using a previously reported procedure.[17] Briefly, Au-poly[$C_{10}VIm^+$][Cl^-] was prepared by combining the IL monomer, 1-decyl-3-vinylimidazolium chloride, [$C_{10}VIm^+Cl^-$], with an aqueous solution of $HAuCl_4$ (achieving H_2O content of 15 ± 1% (w/w)) followed by UV irradiation (λ = 254 nm, 1.5−2 h). Photo irradiation (UV) initiates the polymerization/crosslinking of the vinyl moieties on the IL cation and also reduces Au^{3+} to Au^0 NPs (Figure 1A). The amount of Au NPs (Au NP filling fraction) within the polymer is readily adjusted by controlling the concentration of $AuCl_4^-$ in the self-assembled physical gel prior to UV irradiation.[17] The polymer is durable (self-supporting) and nanostructured (hexagonal perforated lamellar, HPL) with encapsulated Au NPs organized within the hydrophilic pores of the HPL architecture (Figure 1B).[17] The synthesized cylindrical-shaped Au-poly[$C_{10}VIm^+$][Cl^-] were fabricated into an electrode by inserting small segments into a glass capillary and attaching a wire with conductive Ag paste (Figure 1C).[18] The assembly is sealed with insulating (nitrocellulose) cement. Prior to use, each electrode was tested

by cyclic voltammetry (CV) to determine the integrity of the electrical connection. As noted previously, the polymer swells reversibly in water and organic solvents (see Figure S1 in the Supporting Information).[16] Freshly prepared electrodes and aged electrodes stored in water exhibited the same electrochemical activity. However, drying of the polymer causes shrinkage, which results in breaking the electrical contact, serving to stop electrochemical detection.

The electrochemical properties of Au-poly[$C_{10}VIm^+$][Cl^-] electrodes, prepared with an intermediate concentration (0.20 μmoles) of $AuCl_4^-$, were evaluated by cyclic voltammetry (CV), using common anionic and cationic redox probes.[18] The CV curve collected using an anionic redox probe, 20 mM ferrocyanide,[19] $[Fe(CN)_6]^{4-}$, (in 100 mM KCl; scan rate of 25 mV s^{-1}), is presented in Figure 2A (black curve). The forward

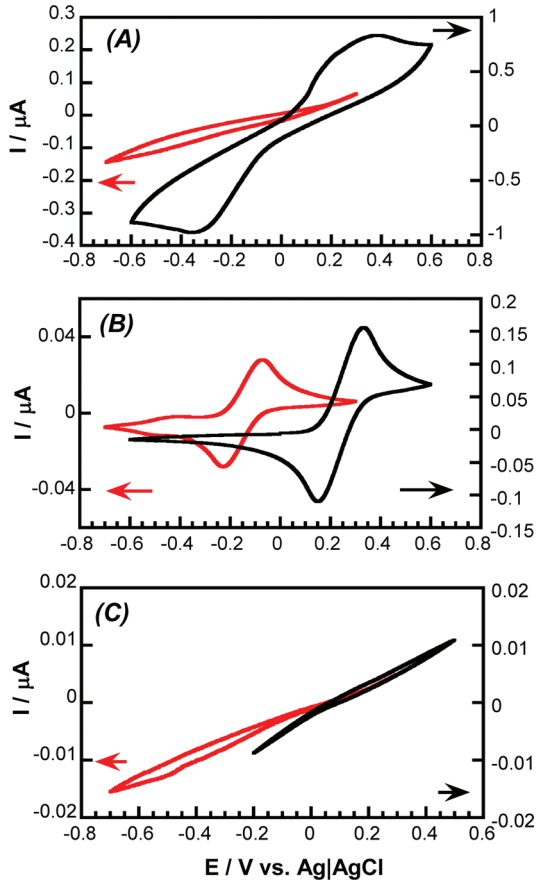

Figure 2. Cyclic voltammograms of 20 mM potassium ferrocyanide, $K_4[Fe(CN)_6]$ (black curves) and 5 mM ruthenium hexamine chloride, $[Ru(NH_3)_6]Cl_3$ (red curves) in 100 mM KCl collected using (A) a Au-poly[$C_{10}VIm^+$][Cl^-] composite electrode (prepared with 0.97 μmol of Au^{3+} in the precursor solution), (B) planar gold disc electrode, or (C) poly[$C_{10}VIm^+$][Cl^-] all collected with a scan rate of 25 mV/s.

scan shows a single broad, plateau-shaped peak at E_{ox} = 0.38 V (vs. Ag/AgCl), signaling the oxidation of Fe^{+2} to Fe^{+3}. The reverse scan shows the corresponding reduction peak at E_{red} = −0.34 V (vs. Ag/AgCl). For comparison, the voltammogram collected on the Fe^{+2}/Fe^{+3} redox couple using a bare Au disc electrode is shown in Figure 2B, black curve. The expected reversible redox process (E_{ox} = 0.33 V and E_{red} = 0.14 V (vs. Ag/AgCl)) with a peak separation and shape consistent with diffusion-limited ion transport through an electrolyte is observed. The increased peak separation for the Fe^{+2}/Fe^{+3} redox couple collected using the Au-poly[$C_{10}VIm^+$][Cl^-] composite electrode (vs. the bare Au electrode) signals significant changes in mass transfer characteristics (i.e., retarded ion permeability), arising from the polymer. Further noted is the non-ideal peak shape (plateau) in the CV collected with the Au-poly[$C_{10}VIm^+$][Cl^-] composite electrode, suggesting convergent ion diffusion possibly through an array of pores.[20] It is noted that the anodic peak currents do not increase linearly with increasing scan rate (see Figure S2 in the Supporting Information), suggesting the electron transfer process between $[Fe(CN)_6]^{4-}$ and the Au-poly[$C_{10}VIm^+$][Cl^-] is not surface confined but rather is a diffusion controlled electrochemical process.[21] Lastly, the oxidation peak shifts to lower potentials with increasing $[Fe(CN)_6]^{4-}$ concentration (20 mM $[Fe(CN)_6]^{4-}$ Figure 2 vs. 100 mM $[Fe(CN)_6]^{4-}$ in Figure S2A in the Supporting Information), indicating that the ion contributing to the redox reaction determines the polarity of the potential shift, a phenomenon often observed in polymers that undergo electrochemomechanical deformations.[22]

The voltammogram collected using a common cationic redox probe, 5 mM $[Ru(NH_3)_6]^{3+}$, (in 100 mM KCl; scan rate of 25 mV s^{-1}), and the Au-poly[$C_{10}VIm^+$][Cl^-] electrode is presented in Figure 2A (red curve). The voltammogram is featureless, indicating that the redox process is effectively inhibited. For comparison, the voltammogram collected using a bare Au electrode is shown in Figure 2B (red curve) and shows the expected E_{ox} = −0.076 V (vs Ag/AgCl) and E_{red} = −0.23 V (vs. Ag/AgCl). Thus, Au-poly[$C_{10}VIm^+$][Cl^-] is anion-permselective, allowing the electrochemical process of the negatively charged redox species ($[Fe(CN)_6]^{4-}$) but inhibiting the positively charged redox probe ($[Ru(NH_3)_6]^{3+}$). Ion permselectivity with polyelectrolytes,[23] chemically-functionalized membranes[24] and mesoporous silicas[25] has been noted previously and is due to the electrostatic interaction between the surface and the redox probe molecules being either attractive or repulsive.[26] Here, the positive charge on the imidazolium-bearing polymer electrostatically attracts anions and is not well-screened by the chloride present in the supporting electrolyte.

To establish the importance of the encapsulated Au NPs within the Au-poly[$C_{10}VIm^+$][Cl^-] composite for electrochemical detection, identical CV experiments were performed using electrodes fabricated solely from poly[$C_{10}VIm^+$][Cl^-], that is using polymer lackingAu NPs. Representative CVs collected using both the anionic and cationic redox probes are presented in Figure 2C and are featureless, indicating the absence of an electrochemical response. This observation clearly indicates the Au NPs are essential for electronic transport. Previously, electrochemical impedance spectroscopy (EIS) and dc conductivity measurements showed that both ionic and electronic transport scales with increasing Au NP content within the poly[$C_{10}VIm^+$][Cl^-].[17] That is, the organized Au NPs within the hydrophilic channels of the HPL structured polymer behave as conduction pathways or electrical conduits. Others have shown in layer-by-layer (LBL) films that the charge transport properties can be varied from electronic charge hopping to bulk conductivity depending on the polyelectrolyte structure, nanoparticle morphology, and self-assembly method used in preparation of the films.[27]

The electrochemical activity of a well-characterized, model homodimeric oxidoreductase, glucose oxidase (GOx) from *Aspergillus niger* was studied. GOx contains two molecules of flavin adenine dinucleotide (FAD), which efficiently catalyzes

the oxidation of glucose generating hydrogen peroxide (H_2O_2). Direct ET is difficult to achieve with GOx because of the buried (recessed) FAD.[28] The shortest distance between the FAD cofactor isoalloxazine ring and the GOx surface is 13 Å.[29] A common method for the immobilization of water-soluble enzymes on solid substrates, such as an electrode, is through simple electrostatic interaction between oppositely charged species.[30] This approach, while not permitting precise control of protein orientation, is extremely simple, offering facile construction. Electrostatic immobilization of GOx onto the Au-poly[$C_{10}VIm^+$][Cl^-] electrode was achieved by soaking the electrode in a buffered aqueous solution of GOx (10 mg/mL in 10 mM phosphate buffer, pH 7.4) overnight at 4 °C. Under these conditions the negatively charged GOx (pI = 4.2) is electrostatically attracted to the positively charged poly-[$C_{10}VIm^+$][Cl^-]. Successful physisorption of the GOx onto the poly(IL) was determined, in part by stripping the adsorbed GOx with 8 M urea in 10 mM phosphate buffer, pH 7.4 and assaying with fluorescence spectroscopy the amount of GOx recovered (see Figure S3 in the Supporting Information).[31] Fluorescence spectroscopy determined that the average surface coverage was $2.70 \pm 0.08 \times 10^{-9}$ mol/cm^2, a value comparable with those reported using a similar electrostatic driven adsorption procedure.[31] The experimental surface coverage of GOx is higher than the theoretical monolayer coverage (4.6×10^{-10} mol/cm^2), suggesting the electrostatic immobilization procedure promotes multilayer coverage.[32]

The integrity of the global secondary structure of the physisorbed enzyme on the Au-poly[$C_{10}VIm^+$][Cl^-] composite was monitored by ATR/FT-IR spectroscopy (Figure 3).[33] The

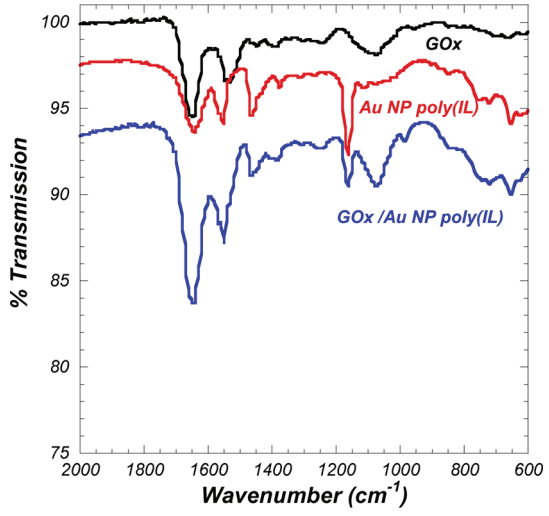

Figure 3. ATR/FT-IR spectra of GOx (black curve), Au-poly-[$C_{10}VIm^+$][Cl^-] composite, prepared with 0.97 μmol of Au^{3+} in the precursor solution, (red curve) and GOx/Au-poly[$C_{10}VIm^+$][Cl^-] composite (blue curve).

amide I (C═O stretching) mode, characteristic of the protein α-helix structure, is observed at 1650 cm^{-1} (Figure 3, blue curve) and compares well with that recorded for the enzyme alone (Figure 3, black curve). The mode at 1637 cm^{-1} (imidazolium) arises from the supporting matrix (Figure 3, red curve).[16] The amide II mode at 1537 cm^{-1} is observed as a shoulder on the imidazolium ring in-plane symmetric/anti-symmetric stretching mode at 1553 cm^{-1}. The amide III mode is clearly visible at 1242 cm^{-1}. In addition, the C–H bending CH_3 and C═O mode are observed at 1389 and 1066 cm^{-1}, respectively. Thus, based upon the spectroscopic studies, the cationic poly(IL) serves as an ideal material promoting the electrostatic adsorption of the negatively charged protein without gross loss of secondary structure.

Evaluation of DET between the adsorbed GOx and the Au-poly[$C_{10}VIm^+$][Cl^-] electrode prepared with high gold content (1.6 μmoles Au^{3+}) was carried out under anaerobic conditions (N_2 saturated electrolyte), Figure 4A (red curve). Two redox

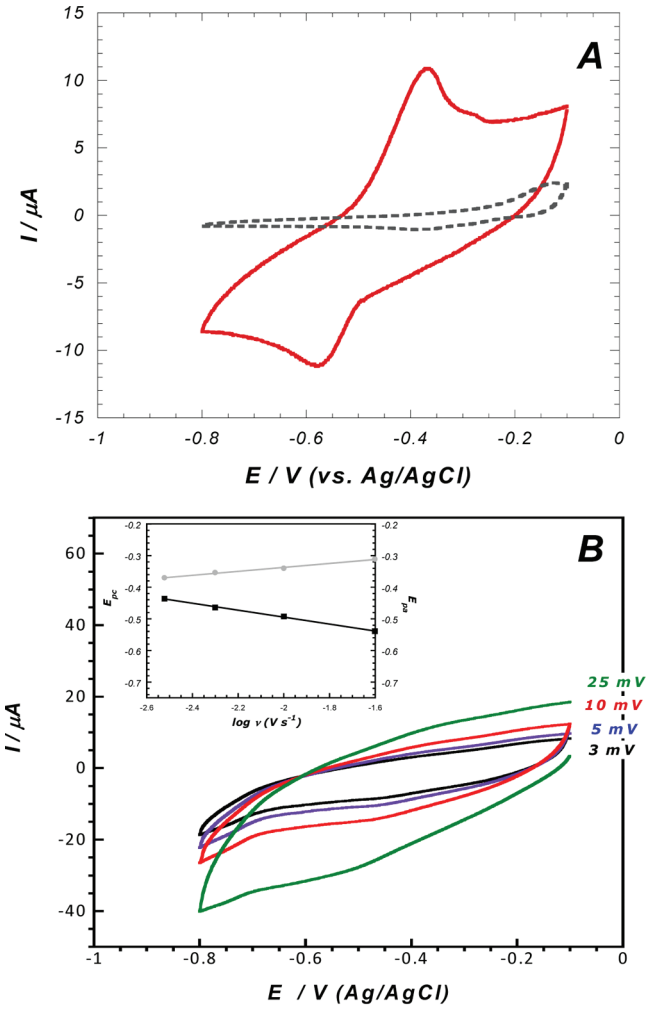

Figure 4. (A) Cyclic voltammograms of the Au-poly[$C_{10}VIm^+$][Cl^-] composite electrode with higher gold content (prepared using 1.60 μmol of Au^{3+} in the precursor solution) with no GOx (black curve) and with GOx (red curve). Measurements were made in 100 mM (N_2 sparged) phosphate buffer (pH 7.1) at 5 mV/s. (B) Cyclic voltammograms of GOx immobilized Au-poly[$C_{10}VIm^+$][Cl^-] composite electrode with low gold content (0.20 μmole Au^{3+}) in 100 mM (N_2 sparged) phosphate buffer (pH 7.1) collected at various scan rates as labeled on graph. Inset: Plot of anodic (gray) and cathodic (black) peak potential dependence with scan rate.

peaks are observed in the CV of the GOx/Au-poly[$C_{10}VIm^+$]-[Cl^-] composite, with a cathodic peak potential (E_{pc}) of −0.58 V (vs. Ag/AgCl)) and an anodic peak (E_{pa}) of −0.37 V (vs. Ag/AgCl), Figure 4A (red curve). The CV of a Au-poly[$C_{10}VIm^+$]-[Cl^-] electrode without adsorbed GOx is featureless within the −0.80 → −0.10 V electrochemical window, Figure 4A, gray curve. The appearance of the redox couple upon GOx adsorption suggests that electrochemically active (i.e., non-

denatured) enzyme is present on the Au-poly[$C_{10}VIm^+$][Cl^-] electrode. (CVs comparing the electrochemical response of GOx/Au-poly[$C_{10}VIm^+$][Cl^-] vs. GOx/poly[$C_{10}VIm^+$][Cl^-] under anaerobic conditions is presented in Figure S4 in the Supporting Information). The formal potential (E^0), determined by averaging the cathodic and anodic peak potentials is −0.472 V (vs. Ag/AgCl, saturated KCl), a value that agrees well with the standard electrode potential of FAD/$FADH_2$ recorded for strongly electrode interacting GOx.[34] The separation of anodic and cathodic peak potentials (ΔE_p) is 197 mV, consistent with quasi-reversible electron transfer.[35,36] The apparent electron transfer rate constant (k_s), determined by Laviron's model,[37] is 0.030 s^{-1}. On the basis of the determined k_s, the average distance for DET was estimated at 23 Å. The electron transfer kinetics and distance determined here is within the theoretical and experimental range expected for redox proteins electrostatically-bound to self-assembled monolayer coated electrodes.[38] Studies performed on composite electrodes prepared with low content of Au^{3+} (0.20 μmoles) produced a less discernible signal, but the CVs possess smaller peak separations, for example, ΔE_p = 68 mV at a scan rate of 10 mV s^{-1}, (Figure 4B). Here, the apparent electron transfer rate constant is 0.312 s^{-1}, indicating faster electron transfer and a value comparable to that reported employing carbon (nanotubes and graphene)-based electrodes.[39] This rate constant also predicts a shorter (20 Å) distance between FAD and the electrode. It was further determined that the peak height varies linearly with the scan rate, indicative of a surface-confined redox couple (Figure 4B, inset).[18] The observed direct electron transfer is believed to arise from surface accessible Au NPs, an observation consistent with recent reports demonstrating that metal nanoparticles can achieve DET and enhance electronic conduction to hemeproteins, metalloenzymes, and photoactive membrane proteins.[40−42] Here, DET may be facilitated by a combination of factors including surface roughness of the polymer composite, exposed Au NPs, and surface deformation (without denaturation of the GOx). The increased electron transfer rate for the electrode prepared with the highest Au^{3+} content is unclear but may be due to Au NP mediated changes in GOx orientation. That is, the composite electrode prepared with 1.6 μmole Au^{3+} would be expected to have a higher density of negatively charged Au NPs[43] compared to the more polycationic rich electrode prepared with 0.97 μmole Au^{3+}. An increase in negatively charged Au NPs would cause the GOx to adjust its orientation, favoring electrostatic interaction with positively charged surface amino acid residues on the protein exterior. Thus, although increased Au NP loading level within the electrode improves electrochemical signal (via enhanced electron transport through the polymer[17]) it can be detrimental to electronic communication to the redox protein. Further enhancement of the rate constant may be achievable through control of protein orientation or by solvent tuning the polymer porosity, thereby increasing exposure of the Au NPs and will be the focus of future studies.

The electro-oxidative properties of the physisorbed GOx were also evaluated by cyclic voltammetry. GOx functions to catalyze the oxidation of glucose to gluconolactone producing H_2O_2 (Figure 5A) and both H_2O_2 and gluconolactone (to gluconic acid) break down spontaneously and catalytically. The CV collected on physisorbed GOx on a Au-poly[$C_{10}VIm^+$][Cl^-] electrode prepared with high gold content (1.6 μmol of Au^{3+}) in the absence of glucose (in air saturated electrolyte) shows the expected cathodic oxygen reduction signal at

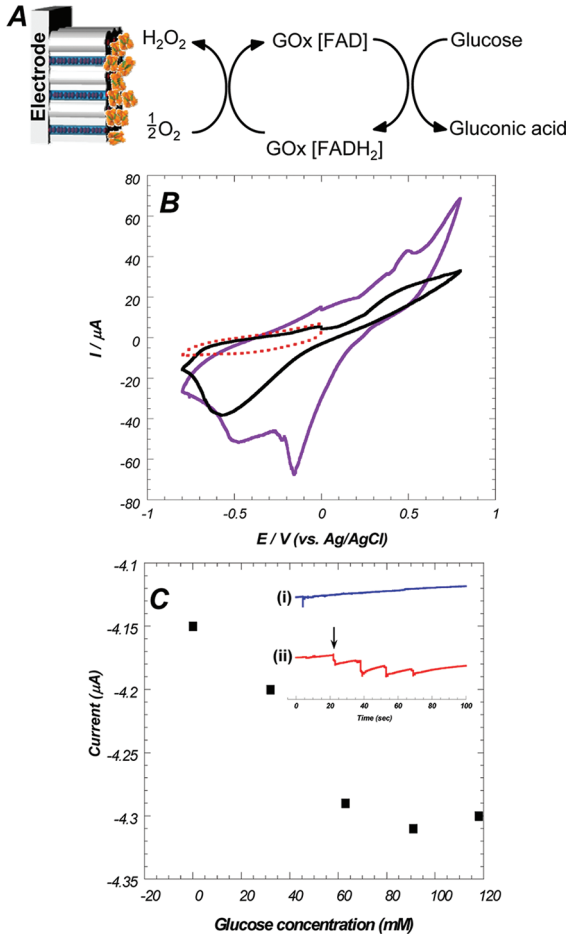

Figure 5. (A) Electrocatalytic scheme for GOx. (B) Cyclic voltammograms of an Au-poly[$C_{10}VIm^+$][Cl^-] composite electrode with higher gold content (prepared using 1.60 μmol of Au^{3+} in the precursor solution) with no GOx (black curve) and with GOx (purple curve) with 25 mM glucose added to the electrolyte (100 mM phosphate buffer (pH 7.1) at 5 mV/s. Measurements were performed in air. For comparison, a CV collected on GOx immobilized Au-poly[$C_{10}VIm^+$][Cl^-] composite electrode with glucose in N_2 sparged 100 mM phosphate buffer (pH 7.1) at 5 mV/s. (red, dashed curve) (C) Glucose calibration curve of GOx/Au-poly[$C_{10}VIm^+$][Cl^-] composite electrode (prepared using 1.60 μmole Au^{3+} in the precursor solution). Inset: current−time curves obtained using Au-poly-[$C_{10}VIm^+$][Cl^-] with GOx (red curve) and with no GOx (blue curve) by the stepwise addition of glucose solution in phosphate buffer at −0.2 V.

potentials less than −0.015 V (Figure 5B, black curve).[44] (For comparison, a CV segment recorded employing N_2 sparged electrolyte is presented in Figure 5B, red, dashed curve). Upon addition of 25 mM glucose, an increase in the anodic current is observed and a discernible peak at 0.47 V (vs. Ag/AgCl) confirms glucose oxidation and formation of gluconolactone and production of H_2O_2 (Figure 5B, purple curve).[45] Data evaluating the response upon addition of higher glucose concentrations (50 mM and 100 mM) were found to generate a further increase in the anodic current (data not shown). The cathodic scan further confirms the production of H_2O_2 by the appearance of reduction features at −0.16 and −0.49 V (vs. Ag/AgCl).[28] These results demonstrate that physisorbed GOx remains electrocatalytically active on the Au-poly[$C_{10}VIm^+$][Cl^-] electrode.

The synergistic electrocatalytic effect of nanoparticles with enzymatically generated H_2O_2 has been reported and shown to enhance sensing by lowering overpotential and reducing interference with other oxidizable compounds.[46,47] Initial studies evaluating the electrocatalytic activity of the Au NPs entrained within the polymeric ionic liquid towards H_2O_2 were performed. CVs comparing the response of a Au-poly-$[C_{10}VIm^+][Cl^-]$ electrode in the absence and presence of 200 mM H_2O_2 are presented in the Supporting Information (Figure S5). The addition of H_2O_2 causes a modest increase in anodic and cathodic currents. The absence of a larger response may arise from the presence of surface adsorbates on the Au NPs (i.e., polymer), since prior work has reported inhibition of electrocatalytic activity towards H_2O_2 due to surface coatings.[48] Future efforts directed at increasing the exposure of the Au NPs (e.g., swelling the composite) will be explored as a means to improve Au-poly$[C_{10}VIm^+][Cl^-]$ for use in biosensing applications.

The amperometric response of a GOx/Au-poly$[C_{10}VIm^+][Cl^-]$ electrode towards the detection of glucose was examined by monitoring the current at an applied potential of −0.2 V (Figure 5C, inset). In contrast to the bare electrode (Au-poly$[C_{10}VIm^+][Cl^-]$) where no electrochemical signal is detected, the reduction current rapidly changes (2−3 s) upon addition of glucose to the electrolyte, indicating electrocatalytic behavior and fast electron exchange behavior of the Au-poly$[C_{10}VIm^+][Cl^-]$ composite electrode. The reductive current response is nonlinear above 91 mM glucose due to saturation of the enzyme active sites.[49] Within the linear response region, the apparent rate constant (K_m) can be determined employing the Lineweaver-Burk equation, $1/i_{ss} = (K_m/i_{max})(1/C) + 1/i_{max}$, where i_{ss} is the steady-state current after addition of substrate, i_{max} is the maximum current under saturated substrate conditions and C is the concentration of the substrate. The determined K_m is 1.23 mM, a value considerably smaller than that reported for GOx in solution (22 mM)[50] but similar to that determined for GOx supported on Au/poly-3-(3-*N*,*N*-diethylaminopropoxyl)thiophene-SWNT composites.[51] Lastly, amperometric steady state i-t curves generated using standard solutions of glucose indicated a detection limit of ca. 1 mM (data not shown). Undoubtedly, this value could be improved with further optimization of the system.

The electrocatalyic effect of Au NPs has been reported previously in a variety of constructs,[52] including those prepared by direct covalent coupling of Au nanoparticles to an enzyme redox center.[9] More recently Holland et al. genetically modified GOx to introduce a reactive thiol moiety that was reacted with a maleimide modified Au NP that enabled direct electrical communication to the electrode surface.[53] Here, we observed electrical communication between the physisorbed enzyme and the Au NP − polymer composite, suggesting that Au-poly$[C_{10}VIm^+][Cl^-]$ functions both as a wire and a bulk electrode.

In summary, this work demonstrates the straightforward fabrication and use of a durable Au NP − polymer hybrid as a conducting biocompatible conduit. The Au NPs localized within the hydrophilic ordered pores of the perforated lamellae form columns that connect the stacked sheets, imparting electronic conductivity to the polyelectrolyte (Figure 1B). The open porous structure allows for electrolyte accessibility and exposure of the Au nanoparticles facilitating DET to the adsorbed enzyme. The polycationic nature of the polymer promotes the selective electrostatic adsorption of the negatively charged enzyme to the electrode at neutral pH. Future work will explore the long-term electrochemical stability of the electrostatically adsorbed enzyme and how solvent swelling of the polyelectrolyte electrode can be used to regulate electrochemical activity, offering a means by which to turn "on" or "off" bioelectrocatalytic functioning. Ultimately, the Au NP−polymer composite may serve as a platform for the fabrication of a wide range of bioelectronic devices, including the construction of a biofuel cell.

■ ASSOCIATED CONTENT

Supporting Information

Volumetric swelling studies, scan rate-dependent CVs of $[Fe(CN)_6]^{4-}$ redox probe with composite and FAD fluorescence emission spectra, CVs comparing DET on Au and no Au composites, and CVs examining electrocatalytic effect of Au NPs. This material is available free of charge via the Internet at http://pubs.acs.org.

■ AUTHOR INFORMATION

Corresponding Author

*Phone: 630-252-8298. Fax: 630-252-9151. E-mail: firestone@anl.gov.

Present Address

[†]Rexam Beverage Can, 700 Corporate Grove Rd., Buffalo Grove, IL 60089

Notes

The authors declare no competing financial interest.

■ ACKNOWLEDGMENTS

This work was supported by the Office of Basic Energy Sciences, Division of Materials Sciences, United States Department of Energy, under Contract DE-AC02-06CH11357 to the UChicago, LLC.

■ REFERENCES

(1) Wallace, G. G.; Kane-Maguire, L. A. P. *Adv. Mater.* **2002**, *14*, 953−960.
(2) Baba, A.; Taranekar, P.; Ponnapati, R. R.; Knoll, W.; Advincula, R. C. *Acs Appl. Mater. Interfaces* **2010**, *2*, 2347−2354.
(3) Bartlett, P. N.; Astier, Y. *Chem. Commun.* **2000**, 105−112.
(4) Armstrong, F. A.; Hill, H. A. O.; Walton, N. J. *Acc. Chem. Res.* **1988**, *21*, 407−413.
(5) Kannan, A. M.; Renugopalakrishnan, V.; Filipek, S.; Li, P.; Audette, G. F.; Munukutla, L. *J. Nanosci. Nanotechnol.* **2009**, *9*, 1665−1678.
(6) Cracknell, J. A.; Vincent, K. A.; Armstrong, F. A. *Chem. Rev.* **2008**, *108*, 2439−2461.
(7) Kim, J.; Jia, H.; Wang, P. *Biotechnol. Adv.* **2006**, *24*, 296−308.
(8) Bullen, R. A.; Arnot, T. C.; Lakeman, J. B.; Walsh, F. C. *Biosens. Bioelectron.* **2006**, *21*, 2015−2045.
(9) Xiao, Y.; Patolsky, F.; Katz, E.; Hainfeld, J. F.; Willner, I. *Science* **2003**, *299*, 1877−1881.
(10) Katz, E.; Sheeney Haj, I.; Willner, I. *Angew. Chem., Int. Ed.* **2004**, *43*, 1877−1881.
(11) Guiseppi-Elie, A.; Lei, C. H.; Baughman, R. H. *Nanotechnology* **2002**, *13*, 559−564.
(12) Tsai, T. W.; Heckert, G.; Neves, L. F.; Tan, Y. Q.; Kao, D. Y.; Harrison, R. G.; Resasco, D. E.; Schmidtke, D. W. *Anal. Chem.* **2009**, *81*, 7917−7925.
(13) Green, O.; Grubjesic, S.; Lee, S. W.; Firestone, M. A. *Polym. Rev.* **2009**, *49*, 339−360.
(14) Zhang, Q.; Lv, X.; Qiao, Y.; Zhang, L.; Liu, D. L.; Zhang, W.; Han, G. X.; Song, X. M. *Electroanal.* **2010**, *22*, 1000−1004.

(15) Lee, S.; Becht, G. A.; Lee, B.; Burns, C. T.; Firestone, M. A. *Adv. Funct. Mater.* **2010**, *20*, 2063−2070.
(16) Batra, D.; Seifert, S.; Varela, L. M.; Liu, A. C. Y.; Firestone, M. A. *Adv. Funct. Mater.* **2007**, *17*, 1279−1287.
(17) Lee, S.; Cummins, M. D.; Willing, G. A.; Firestone, M. A. *J. Mater. Chem.* **2009**, *19*, 8092−8101.
(18) Wu, X. M.; Zhao, B.; Wu, P.; Zhang, H.; Cai, C. X. *J. Phys. Chem. B* **2009**, *113*, 13365−13373.
(19) Pardo-Yissar, V.; Gabai, R.; Shipway, A. N.; Bourenko, T.; Willner, I. *Adv. Mater.* **2001**, *13*, 1320−1323.
(20) Silva, T. H.; Barreira, S. V. P.; Moura, C. *Port. Electrochim. Acta* **2003**, *21*, 281−292.
(21) Riskin, M.; Basnar, B.; Chegel, V. I.; Katz, E.; Willner, I.; Shi, F.; Zhang, X. *J. Am. Chem. Soc.* **2006**, *128*, 1253−1260.
(22) Takashima, W.; Pandey, S. S.; Kaneto, K. *Thin Solid Films* **2003**, *438-439*, 339−345.
(23) Park, M.-K.; Deng, S.; Advincula, R. C. *J. Am. Chem. Soc.* **2004**, *126*, 13723−13731.
(24) Newton, M. R.; Bohaty, A. K.; White, H. S.; Zharov, I. *J. Am. Chem. Soc.* **2005**, *127*, 7268−7269.
(25) Calvo, A.; Yameen, B.; Williams, F. J.; Soler-Illia, G. J. A. A.; Azzaroni, O. *J. Am. Chem. Soc.* **2009**, *131*, 10866−10868.
(26) Motornov, M.; Tam, T. K.; Pita, M.; Tokarev, I.; Katz, E.; Minko, S. *Nanotechnol.* **2009**, *20*, 434006.
(27) Ferreyra, N.; Coche-Guerente, L.; Fatisson, J.; Lopez Teijelo, M.; Labbe, P. *Chem. Commun.* **2003**, 2056−2057.
(28) Rakhi, R. B.; Sethupathi, K.; Ramaprabhu, S. *J. Phys. Chem. B* **2009**, *113*, 3190−3194.
(29) Liu, J. Q.; Paddon-Row, M. N.; Gooding, J. J. *J. Phys. Chem. B* **2004**, *108*, 8460−8466.
(30) Muguruma, H.; Kase, Y.; Murata, N.; Matsumura, K. *J. Phys. Chem. B* **2006**, *110*, 26033−26039.
(31) Akhtar, M. S.; Ahmad, A.; Bhakuni, V. *Biochemistry* **2002**, *41*, 7142−7149.
(32) Otsuka, I.; Yaoita, M.; Nagashima, S.; Higano, M. *Electrochim. Acta* **2005**, *50*, 4861−4867.
(33) Portaccio, M.; Della Ventura, B.; Mita, D.; Manolova, N.; Stoilova, O.; Rashkov, I.; Lepore, M. *J. Sol-Gel Sci. Tech.* **2011**, *57*, 204−211.
(34) Courjean, O.; Gao, F.; Mano, N. *Angew. Chem. Inter. Ed.* **2009**, *48*, 5897−5899.
(35) Zhang, Y.; Chen, X.; Wang, J.; Yang, W. *Electrochem. Solid-State Lett.* **2008**, *11*, F19−F21.
(36) Wang, Z.; Liu, S.; Wu, P.; Cai, C. *Anal. Chem.* **2009**, *81*, 1638−1645.
(37) Laviron, E. *J. Electroanal. Chem.* **1979**, *101*, 19−28.
(38) Georg, S.; Kabuss, J.; Weidinger, I. M.; Murgida, D. H.; Hildebrandt, P.; Knorr, A.; Richter, M. *Phys. Rev. E* **2010**, *81*, 046101.
(39) Kang, X.; Wang, J.; Wu, H.; Aksay, I. A.; Liu, J.; Lin, Y. *Biosens. Bioelectron.* **2009**, *25*, 901−905.
(40) Abad, J. M.; Gass, M.; Bleloch, A.; Schiffrin, D. J. *J. Am. Chem. Soc.* **2009**, *131*, 10229−10236.
(41) Jensen, P. S.; Chi, Q.; Grumsen, F. B.; Abad, J. M.; Horsewell, A.; Schiffrin, D. J.; Ulstrup, J. *J. Phys. Chem. C* **2007**, *111*, 6124−6132.
(42) Ron, I.; Friedman, N.; Sheves, M.; Cahen, D. *J. Phys. Chem. Lett.* **2010**, *1*, 3072−3077.
(43) Zhong, Z. Y.; Patskovskyy, S.; Bouvrette, P.; Luong, J. H. T.; Gedanken, A. *J. Phys. Chem. B* **2004**, *108*, 4046−4052.
(44) Plumere, N.; Henig, J.; Campbell, W. H. *Anal. Chem.* **2012**, *84*, 2141−2146.
(45) Yu, J. J.; Lu, S.; Li, J. W.; Zhao, F. Q.; Zeng, B. Z. *J. Solid State Electrochem.* **2007**, *11*, 1211−1219.
(46) Kang, X. H.; Mai, Z. B.; Zou, X. Y.; Cai, P. X.; Mo, J. Y. *Anal. Biochem.* **2007**, *369*, 71−79.
(47) Vijayalakshmi, A.; Karthikeyan, R.; Berchmans, S. *J. Phys. Chem. C* **2010**, *114*, 22159−22164.
(48) Das, J.; Patra, S.; Yang, H. *Chem. Commun.* **2008**, 4451−4453.
(49) Guascito, M. R.; Chirizzi, D.; Malitesta, C.; Mazzotta, E. *Analyst* **2011**, *136*, 164−173.
(50) Wang, B.; Li, B.; Deng, Q.; Dong, S. *Anal. Chem.* **1998**, *70*, 3170−3174.
(51) Pang, X.; Imin, P.; Zhitomirsky, I.; Adronov, A. *Macromolecules* **2010**, *43*, 10376−10381.
(52) Zabet-Khosousi, A.; Dhirani, A.-A. *Chem. Rev.* **2008**, *108*, 4072−4124.
(53) Holland, J. T.; Lau, C.; Brozik, S.; Atanassov, P.; Banta, S. *J. Am. Chem. Soc.* **2011**, *133*, 19262−19265.